Diffusion Synthetic Acceleration (DSA) for the Linear Discontinuous Expansion Method with Subcell Balance (LDEM-SCB)

Habib Muhammad, Ser Gi Hong*
Department of Nuclear Engineering, Kyung Hee University: 1732 Deogyeong-daero, Giheung-gu, Yongin, Gyeonggi-do, 446-701, Korea
**Corresponding author: sergihong@khu.ac.kr*

1. Introduction

Many areas in nuclear engineering require the accurate solutions of the radiation transport equations for complicated geometrical problems. The treatment of the complicated geometries using deterministic methods requires the use of unstructured meshes such as tetrahedral meshes. Recently, there have been significant efforts to devise the accurate spatial discretization methods for the multi-group Boltzmann transport equation in the complicated geometrical problems [1]. For example, the discontinuous finite elements method (DFEM) was implemented in Multi-group Unstructured geometry S_N Transport code (MUST) and new sub-cell balance methods with linear discontinuous expansion were developed and implemented in the code MUST [2].

It is well known that the iteration solutions of the transport equations converge very slowly in high scattering dominant regions. Therefore, there have been lots of research works to develop acceleration methods to reduce computing time. One of them, DSA (Diffusion Synthetic Acceleration) is a very powerful method to accelerate the convergence of the SI (source iteration) method. However, the development of an efficient DSA is a critical issue in the numerical methods for solving the transport equation for the complicated geometries. The present work is aimed at developing and implementing the DSA equations for the subcell balance method LDEM-SCB(1) in unstructured tetrahedral meshes used in the MUST code and analyzing it for 3D problem. In this work, the discretized DSA equations are developed by consistently discretizing the continuous diffusion equation with LDEM-SCB(1).

2. Methods and Results

2.1. Derivation of the Continuous DSA Equations

It starts by describing diffusion synthetic acceleration (DSA) applied to an analytic transport problem with one energy group. Without acceleration, the source iteration procedure for the transport equation with isotropic scattering can be described by

$$\hat{\Omega}.\nabla\Psi^{(l+\frac{1}{2})}+\sigma_t\Psi^{(l+\frac{1}{2})}=\frac{\sigma_s}{4\pi}\phi^{(l)}+q\,, \tag{1}$$

$$\phi^{(l)}\equiv\phi^{(l+\frac{1}{2})}\equiv\int_{4\pi}d\hat{\Omega}\Psi^{(l+\frac{1}{2})}, \tag{2}$$

where Ψ and ϕ represent the angular flux and scalar flux, respectively, and ℓ the iterative index for the source iteration.

The SI scheme converges very slowly in high scattering dominant and optically thick region problems. To derive the DSA equations, taking zeroth and first angular moments of Eq. (1) given by

$$\begin{aligned}&\nabla\Phi_1^{(l+\frac{1}{2})}+\sigma_t\phi^{(l+\frac{1}{2})}=\sigma_s\phi^{(l)}+q_0\,,\\&\frac{1}{3}\nabla\phi^{(l+\frac{1}{2})}+\frac{2}{3}\nabla\Phi_2^{(l+\frac{1}{2})}+\sigma_t\Phi_1^{(l+\frac{1}{2})}=q_1\,,\end{aligned} \tag{3}$$

where the angular moments are defined by

$$\begin{aligned}&\Phi_1^{(l+\frac{1}{2})}=current\ vector=\int_{4\pi}d\hat{\Omega}\hat{\Omega}\Psi^{(l+\frac{1}{2})},\\&\Phi_2^{(l+\frac{1}{2})}=2^{nd}order\ moment\ tensor=\int_{4\pi}d\hat{\Omega}\frac{1}{2}\left(3\hat{\Omega}\hat{\Omega}-I\right)\hat{\Omega}\Psi^{(l+\frac{1}{2})}.\end{aligned} \tag{4}$$

In Eq. (3), all the iteration indices except for $\Phi_2^{(l+\frac{1}{2})}$ are changed into (ℓ+1) to obtain the diffusion equation for acceleration [3], which gives

$$\begin{aligned}&\nabla\Phi_1^{(l+1)}+\sigma_t\phi^{(l+1)}=\sigma_s\phi^{(l+1)}+q_0\,,\\&\frac{1}{3}\nabla\phi^{(l+1)}+\frac{2}{3}\nabla\Phi_2^{(l+\frac{1}{2})}+\sigma_t\Phi_1^{(l+1)}=q_1\,.\end{aligned} \tag{5}$$

The subtraction of Eq. (3) from Eq. (5) gives the following diffusion equations:

$$\begin{aligned}&\nabla.\vec{F}^{(l+1)}+\sigma_a f^{(l+1)}=\sigma_s\left(\phi^{(l+\frac{1}{2})}-\phi^{(l)}\right),\\&\frac{1}{3}\nabla f^{(l+1)}+\sigma_t\vec{F}^{(l+1)}=0\,,\end{aligned} \tag{6}$$

where the following definitions are given by

$$\begin{aligned}&\vec{F}^{(l+1)}=\Phi_1^{(l+1)}-\Phi_1^{(l+\frac{1}{2})}\,,\\&f^{(l+1)}=\phi^{(l+1)}-\phi^{(l+\frac{1}{2})}\,,\end{aligned} \tag{7}$$

where $\vec{F}^{(l+1)}$ is the vector current correction and $f^{(l+1)}$ is the scalar flux correction.

After solving the DSA equation, the scalar flux for the next iteration is updated by using the equation:

$$\phi^{(l+1)} = \phi^{(l+\frac{1}{2})} + f^{(l+1)}. \tag{8}$$

2.2 Discretized Form of DSA

As described in section 1, the discretized form of the DSA equation is derived by discretizing the continuous diffusion equation (i.e. Eq. (6)) in a consistent manner as used in the LDEM-SCB(1). This discretization starts with the subcell balance equation of Eq. (6). For example, the subcell balance equation of the first subcell of a tetrahedron cell '*k*' is given by

$$\int_{V_{sc1}} \nabla.\vec{F}^{k,(l+1)} + \int_{V_{sc1}} \sigma_a f^{k,(l+1)} = \int_{V_{sc1}} q^{k,(l+1)}, \tag{9}$$

where $q^{k,(l+1)}$ is the source defined by

$$q^{k,(l+1)} = \sigma_s\left(f_k^{k,(l+\frac{1}{2})} - f_k^{k,(l)} \right). \tag{10}$$

The use of the Green's theorem for Eq. (9) after dropping the iteration index, for simplicity, gives

$$\int_{A_{sc1}} dA\vec{F}^k.\hat{n} + \sigma_a \bar{f}_{sc1}^k V_{sc1}^k = q_{sc1}^k V_{sc1}^k, \tag{11}$$

where $\bar{f}_{sc1}^k$ is the average value of the scalar flux correction over the first subcell of the present cell '*k*' and V_{sc1}^k is volume of the subcell-1.

Equation (11) can be rewritten by decomposing the surface integral into external and interface surface terms as follows:

$$\begin{aligned} &\left(\vec{F}_{1,2}^{k,ef}.\vec{A}_{1,2}^{k,ef} + \vec{F}_{1,3}^{k,ef}.\vec{A}_{1,3}^{k,ef} + \vec{F}_{1,4}^{k,ef}.\vec{A}_{1,4}^{k,ef}\right) \\ &+\left(\vec{F}_{1,2}^{k,if}.\vec{A}_{1,2}^{k,if} + \vec{F}_{1,3}^{k,if}.\vec{A}_{1,3}^{k,if} + \vec{F}_{1,4}^{k,if}.\vec{A}_{1,4}^{k,if}\right) \\ &+\sigma_a^k \bar{f}_{sc1}^k V_{sc1}^k = q_{sc1}^k V_{sc1}^k, \end{aligned} \tag{12}$$

where the superscripts '*ef*' and '*if*' refer to the external and internal faces respectively, and the subscripts in the current corrections and vector areas (see Fig. 1 [2]) refer to the node and face numbers of the tetrahedron '*k*'. For example, $\vec{F}_{1,2}^{k,ef}$ represents the current correction over the external subsurface $\vec{A}_{1,2}^{k,ef}$ in the subcell-1, whereas $\vec{A}_{1,2}^{k,ef}$ represents external face-2 which is opposite to the node-2 in the subcell-1 as shown in Fig. 1.

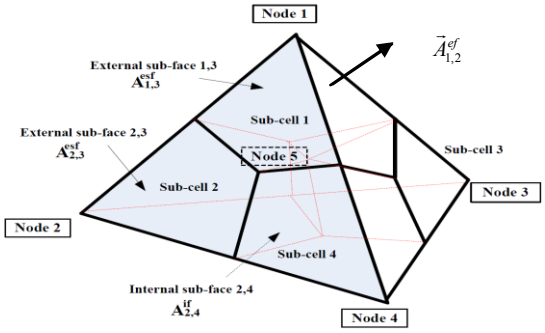

Figure 1: Sub-cell division for LDEM-SCB(1)

For the external subface $\vec{A}_{1,2}^{k,ef}$ in the *k*'th cell, the net current correction is decomposed into the partial current corrections as follows:

$$\begin{aligned} \vec{F}_{1,2}^{k,ef}.\vec{A}_{1,2}^{k,ef} &= \vec{F}_{1,2}^{k,ef}.n_{1,2}^k\left|\vec{A}_{1,2}^{ef}\right| = \left|\vec{A}_{1,2}^{ef}\right|\left(\vec{F}_{1,2}^{k,ef}.n_{1,2}^k\right), \\ \vec{F}_{1,2}^{k,ef}.\vec{A}_{1,2}^{k,ef} &= \frac{1}{3}\left|\vec{A}_2^k\right|\left(\vec{F}_{1,2}^{+,k,ef} - \vec{F}_{\alpha',\beta'}^{+,k(1,2),ef}\right). \end{aligned} \tag{13}$$

where $\vec{F}_{1,2}^{+,k,ef}$ and $\vec{F}_{\alpha',\beta'}^{+,k(1,2),ef}$ represents the outgoing and incoming partial current corrections, respectively, across the external subface $\vec{A}_{1,2}^{k,ef}$ are defined by

$$\vec{F}_{1,2}^{+,k,ef} = \frac{1}{4}f_{1,2}^k - \frac{D^k}{2\left|\vec{A}_2^k\right|}\left(A_{2x}^k\frac{\partial f^k}{\partial x} + A_{2y}^k\frac{\partial f^k}{\partial y} + A_{2z}^k\frac{\partial f^k}{\partial z}\right), \tag{14}$$

$$\vec{F}_{\alpha',\beta'}^{+,k(1,2),ef} = \frac{1}{4}f_{\alpha',\beta'}^{k(1,2)} + \frac{D^{k'}}{2\left|\vec{A}_2^k\right|}\left(A_{2x}^k\frac{\partial f^{k'}}{\partial x'} + A_{2y}^k\frac{\partial f^{k'}}{\partial y'} + A_{2z}^k\frac{\partial f^{k'}}{\partial z'}\right), \tag{15}$$

where $f_{1,2}^k$ is the scalar flux correction over the external subface $\vec{A}_{1,2}^{k,ef}$ in the cell '*k*' and similarly $f_{\alpha',\beta'}^{k(1,2)}$ is the scalar flux correction over its external subface $\vec{A}_{\alpha',\beta'}^{k',ef}$ of the cell 'k'' adjacent to the cell 'k' through subface $\vec{A}_{1,2}^{k,ef}(=-\vec{A}_{\alpha',\beta'}^{k',ef})$ are defined respectively:

$$f_{1,2}^k = \frac{22}{36}f_{p1}^k + \frac{7}{36}\left(f_{p3}^k + f_{p4}^k\right), \tag{16}$$

$$f_{\alpha',\beta'}^{k(1,2)} = \frac{22}{36}f_{p\alpha'}^{k(1,2)} + \frac{7}{36}\left(f_{p\gamma'}^{k(1,2)} + f_{p\delta'}^{k(1,2)}\right) \tag{17}$$

In Eq. (16), f_{pi}^k represents the scalar flux correction at the node '*i*' of the cell '*k*'. To solve Eqs. (14) and (15), we used the barycentric transformation between global coordinates (x,y,z) and local coordinates $(\xi_1,\xi_2,\xi_3,\xi_4)$ systems. Any linear function $g(x,y,z)$ that

takes the values $g_i(i=1,2,3,4)$ at the nodes of a tetrahedron can be represented in terms of the local barycentric coordinates as follows:

$$g(\xi_1,\xi_2,\xi_3,\xi_4)=g_1\xi_1+g_2\xi_2+g_3\xi_3+g_4\xi_4=\sum_{i=1}^{4}g_i\xi_i. \quad (18)$$

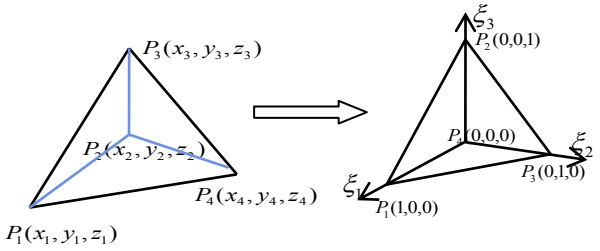

Figure 2: Barycentric coordinates transformation

With the barycentric transformation, the partial current correction over the external subfaces in Eqs. (14) and (15) are calculated and substituted in Eq. (13). The net current is given by

$$\vec{F}^{k,ef}_{1,2}.\vec{A}^{k,ef}_{1,2}=\frac{1}{432}\left\{\begin{array}{l}\left[\begin{array}{l}\left\{22\left|\vec{A}^k_2\right|+\frac{24D_k}{V_k}\left(\vec{A}^k_1.\vec{A}^k_2\right)\right\}f^k_{p1}+\left\{\frac{24D_k}{V_k}\left(\vec{A}^k_2.\vec{A}^k_2\right)\right\}f^k_{p2}\\ \left\{7\left|\vec{A}^k_2\right|+\frac{24D_k}{V_k}\left(\vec{A}^k_1.\vec{A}^k_3\right)\right\}f^k_{p3}+\left\{7\left|\vec{A}^k_2\right|+\frac{24D_k}{V_k}\left(\vec{A}^k_1.\vec{A}^k_4\right)\right\}f^k_{p4}\end{array}\right]\\ -\left[\begin{array}{l}\left|\vec{A}^k_2\right|\left(\frac{22}{36}f^{k'(1,2)}_{p\alpha'}+\frac{7}{36}f^{k'(1,2)}_{p\gamma'}+\frac{7}{36}f^{k'(1,2)}_{p\delta'}\right)\\ -\frac{24D^{k'}}{V^{k'}}\left(\begin{array}{l}\left(\vec{A}^k_2.\vec{A}^{k'}_{\alpha'}\right)f^{k'(1,2)}_{p\alpha'}+\left(\vec{A}^k_2.\vec{A}^{k'}_{\beta'}\right)f^{k'(1,2)}_{p\beta'}\\ +\left(\vec{A}^k_2.\vec{A}^{k'}_{\gamma'}\right)f^{k'(1,2)}_{p\gamma'}+\left(\vec{A}^k_2.\vec{A}^{k'}_{\delta'}\right)f^{k'(1,2)}_{p\delta'}\end{array}\right)\end{array}\right]\end{array}\right\}. \quad (19)$$

Similarly, the one over an internal subface is given by

$$\vec{F}^{k,if}_{1,2}.\vec{A}^{k,if}_{1,2}=\frac{D_k}{36V_k}\left\{\begin{array}{l}\left(\vec{A}^k_2-\vec{A}^k_1\right)\vec{A}^k_1f^k_{p1}+\left(\vec{A}^k_2-\vec{A}^k_1\right)\vec{A}^k_2f^k_{p2}\\ +\left(\vec{A}^k_2-\vec{A}^k_1\right)\vec{A}^k_3f^k_{p3}+\left(\vec{A}^k_2-\vec{A}^k_1\right)\vec{A}^k_4f^k_{p4}\end{array}\right\}. \quad (20)$$

After representing all the internal and external current correction across internal and external faces in terms of point scalar flux corrections and substituting them into Eq. (12) gives the final subcell-1 balance equation.

$$\begin{aligned}&\left\{22\left(\left|\vec{A}^k_2\right|+\left|\vec{A}^k_3\right|+\left|\vec{A}^k_4\right|\right)+\frac{24D_k}{V_k}\left(\vec{A}^k_1.\vec{A}^k_1\right)+225\Sigma^k_aV_{scl}\right\}f^k_{p1}+\left\{7\left(\left|\vec{A}^k_3\right|+\left|\vec{A}^k_4\right|\right)+\frac{24D_k}{V_k}\left(\vec{A}^k_1.\vec{A}^k_2\right)+69\Sigma^k_aV_{scl}\right\}f^k_{p2}\\&+\left\{7\left(\left|\vec{A}^k_2\right|+\left|\vec{A}^k_4\right|\right)+\frac{24D_k}{V_k}\left(\vec{A}^k_1.\vec{A}^k_3\right)+69\Sigma^k_aV_{scl}\right\}f^k_{p3}+\left\{7\left(\left|\vec{A}^k_2\right|+\left|\vec{A}^k_3\right|\right)+\frac{24D_k}{V_k}\left(\vec{A}^k_1.\vec{A}^k_4\right)+69\Sigma^k_aV_{scl}\right\}f^k_{p4}\\&=V_{scl}\left\{225q^k_{p1}+69\left(q^k_{p2}+q^k_{p3}+q^k_{p4}\right)\right\}\\&+\left[\left|\vec{A}^k_2\right|\left\{\frac{22}{36}f^{k'(1,2)}_{p\alpha'}+\frac{7}{36}f^{k'(1,2)}_{p\gamma'}+\frac{7}{36}f^{k'(1,2)}_{p\delta'}\right\}-\frac{24D^{k'(1,2)}}{V^{k'(1,2)}}\left\{\begin{array}{l}\left(\vec{A}^k_2.\vec{A}^{k'}_{\alpha'}\right)f^{k'(1,2)}_{p\alpha'}+\left(\vec{A}^k_2.\vec{A}^{k'}_{\beta'}\right)f^{k'(1,2)}_{p\beta'}\\ +\left(\vec{A}^k_2.\vec{A}^{k'}_{\gamma'}\right)f^{k'(1,2)}_{p\gamma'}+\left(\vec{A}^k_2.\vec{A}^{k'}_{\delta'}\right)f^{k'(1,2)}_{p\delta'}\end{array}\right\}\right]\\&+\left[\left|\vec{A}^k_3\right|\left\{\frac{22}{36}f^{k'(1,3)}_{p\alpha'}+\frac{7}{36}f^{k'(1,3)}_{p\gamma'}+\frac{7}{36}f^{k'(1,3)}_{p\delta'}\right\}-\frac{24D^{k'(1,3)}}{V^{k'(1,3)}}\left\{\begin{array}{l}\left(\vec{A}^k_3.\vec{A}^{k'}_{\alpha'}\right)f^{k'(1,3)}_{p\alpha'}+\left(\vec{A}^k_3.\vec{A}^{k'}_{\beta'}\right)f^{k'(1,3)}_{p\beta'}\\ +\left(\vec{A}^k_3.\vec{A}^{k'}_{\gamma'}\right)f^{k'(1,3)}_{p\gamma'}+\left(\vec{A}^k_3.\vec{A}^{k'}_{\delta'}\right)f^{k'(1,3)}_{p\delta'}\end{array}\right\}\right]\\&+\left[\left|\vec{A}^k_4\right|\left\{\frac{22}{36}f^{k'(1,4)}_{p\alpha'}+\frac{7}{36}f^{k'(1,4)}_{p\gamma'}+\frac{7}{36}f^{k'(1,4)}_{p\delta'}\right\}-\frac{24D^{k'(1,4)}}{V^{k'(1,4)}}\left\{\begin{array}{l}\left(\vec{A}^k_4.\vec{A}^{k'}_{\alpha'}\right)f^{k'(1,4)}_{p\alpha'}+\left(\vec{A}^k_4.\vec{A}^{k'}_{\beta'}\right)f^{k'(1,4)}_{p\beta'}\\ +\left(\vec{A}^k_4.\vec{A}^{k'}_{\gamma'}\right)f^{k'(1,4)}_{p\gamma'}+\left(\vec{A}^k_4.\vec{A}^{k'}_{\delta'}\right)f^{k'(1,4)}_{p\delta'}\end{array}\right\}\right]\end{aligned} \quad (21)$$

The remaining DSA equations for other three subcells are derived in the same manners and finally they give a set of four DSA equations for one cell '*k*'.

3. Numerical Test

The numerical estimation of spectral radius gives an insight of the validity of the solution techniques. So, in this paper, the spectral radii of our DSA were numerically estimated to show the performance for various mesh divisions with the following equation:

$$\rho\approx\frac{\left\|\phi_p^{(l+1)}-\phi_p^{(l)}\right\|_2}{\left\|\phi_p^{(l)}-\phi_p^{(l-1)}\right\|_2}. \quad (22)$$

For all the test problems, the reflective boundary conditions (BCs) were applied to *-x, -y,* and *–z* external faces while vacuum BCs were applied to all other external faces. A uniform external source of 10 #cm^{-3}sec^{-1} is distributed in the region. The scattering ratio c is 0.9999 and the convergence criterion for transport sweep is 1.0×10^{-8} and for DSA is 1.0×10^{-5} for all the test problems.

The first test problem is comprised of a 6×6×6 grid of unit boxes. Each unit box has 2.0cm, 1.0cm and 8.0cm sides along *x, y* and z-axis directions, respectively. Each unit box is divided in six tetrahedrons of equal volume for all the problems.

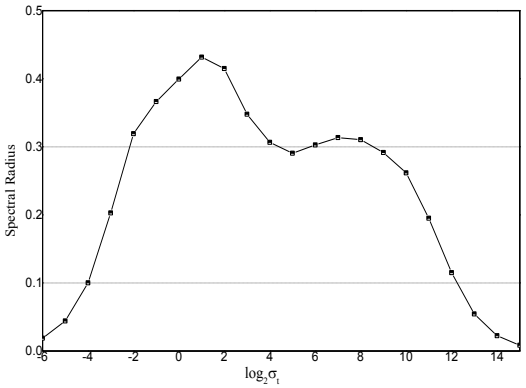

Figure 3: Spectral radius as a function of logarithmic total XS

In Fig. 3, the numerically estimated spectral radius is plotted against the logarithmic total cross section. It shows that over a wide range of total cross section, the solution is converged and the maximum spectral radius is 0.4317 at σ_t=2.7183.

The second test problem comprised of a 10×10×10 grid of unit boxes. Each unit box has 2.0cm, 2.0cm and 2.0cm sides along *x, y* and z-axis directions, respectively.

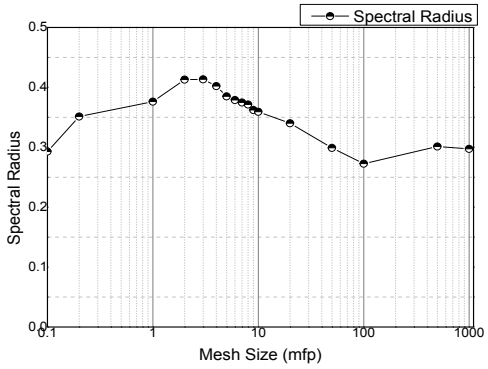

Figure 4: Spectral radius as a function of mesh size (mfp)

In Fig. 4, spectral radius is plotted as a function of mesh size expressed in terms of mean free path (mfp). Fig.4 shows that DSA is converged over a wide range of total XS and the spectral radii are less than 0.42.

The last test problem was considered to test the DSA for various minimum aspect ratios of tetrahedron meshes [4]. Minimum aspect ratio 'α_{min}' is defined as the ratio of three times the radius of the inscribed circle to the radius of circumscribed circle. This problem is comprised of 8×8×8 grid of unit boxes. The dimensions of each unit box are described for various minimum aspect ratios in Table 1. Minimum aspect ratios are tabulated in terms of the dimensions of the basic elements used. The minimum aspect ratio ranges from 0.116 to 0.632 for different dimensions of unit box.

Fig. 5 compares the spectral radii for different DSA methods versus minimum aspect ratio. In terms of spectral radius, FCDSA (Fully Consistent DSA) showed the best performance. Our method showed better performance than the other two methods (i.e., WLA (Wareing, Larsen and Adams) and M4S (Modified Four Steps)). It is also noted that the spectral radius showed only a small variation (~0.4) over all the values of min aspect ratios, which is similar to FCDSA.

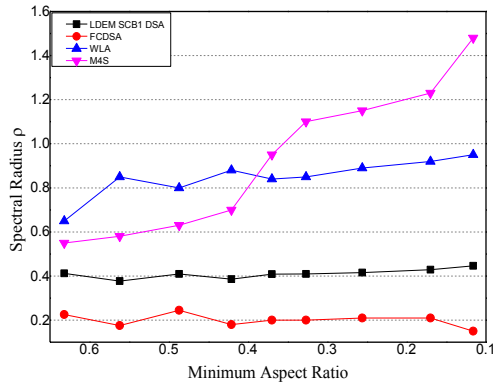

Figure 5: Spectral radius as a function of mini aspect ratio

Table 1: Minimum Aspect Ratio in terms of Dimensions [4]

Δx (cm)	Δy (cm)	Δz (cm)	α_{min}
1.0	1.0	1.0	0.632
2.0	2.0	3.0	0.562
1.0	1.0	2.0	0.487
2.0	2.0	5.0	0.421
2.0	1.0	3.0	0.370
3.0	1.0	3.0	0.327
2.0	1.0	5.0	0.256
2.0	1.0	8.0	0.170
8.0	1.0	10.0	0.116

4. Summary and Conclusion

In this study, a DSA scheme was developed for LDEM-SCB(1) by consistently discretizing the continuous diffusion equation to the derivation used in the LDEM-SCB(1). The numerical estimation of spectral radius for various test problems showed that DSA scheme devised to LDEM-SCB(1) is very effective over wide range of mesh size and optical thickness. In particular our method was very stable for various minimum aspect ratios even if some well-known DSA methods showed degraded spectral radii. This property of our DSA makes it more useful over other DSA schemes. However, it is found that the number of iterations in solving the DSA itself is bit higher and becomes slower when the mesh size (in mfp) is in the range from 2~5. A detailed study is underway to investigate this behaviour and it is hoped that this study will reduce the DSA iterations count and make it more effective and faster to reduce the computing time.

5. References

[1] Todd A. Wareing, *at al*, "Discontinuous Finite Element Sn Methods on Three Dimensional Unstructured Grids", *Nucl. Sci. Eng*., **138,** 256-268 (2001).
[2] S. G. Hong, "Two Subcell Balance Methods for Solving the Multigroup Discrete Ordinates Transport Equation with Tetrahedral Meshes", *Nucl. Sci. Eng*., **173,** 101-117 (2013).
[3] Marvin J. Adams, William R. Martin, "Diffusion Synthetic Acceleration of Discontinuous Finite Element Transport Iterations", *Nucl. Sci. Eng*., **111,** 145-167 (1992).
[4] Warsa JS, Wareing TA, Morel JE, "Fully Consistent Diffusion Synthetic Acceleration of Linear Discontinuous Sn Transport Discretizations on Unstructured Tetrahedral Meshes", *Nucl. Sci. Eng*., 141-236 (2002).